Blast response of laminated glass

A gas-gun experimental investigation of the fracture pattern and yield lines observed in full-scale blast tests

Angelides, S. C.; Talbot, J. P.; Overend, M.

DOI
10.1016/j.compstruct.2023.117286

Publication date
2023

Document Version
Final published version

Published in
Composite Structures

Composite Structures 321 (2023) 117286

Contents lists available at ScienceDirect

Composite Structures

journal homepage: www.elsevier.com/locate/compstruct

Blast response of laminated glass: A gas-gun experimental investigation of the fracture pattern and yield lines observed in full-scale blast tests

S.C. Angelides [a,*,1], J.P. Talbot [a], M. Overend [b]

[a] Department of Engineering, University of Cambridge, Cambridge, UK
[b] Faculty of Architecture and the Built Environment, Delft University of Technology, Delft, the Netherlands

ARTICLE INFO

Keywords:
Laminated glass
Blast response
Inertia loading
Post-fracture
Collapse mechanism
Yield line

ABSTRACT

The applications of architectural and automotive laminated glass continue to grow. This is largely due to the enhanced safety in extreme events, such as blast. However, the complex interaction between the glass fragments and the polymer interlayer after glass fracture is still only partially understood, with existing analysis methods adopting a semi-empirical approach for the post-fracture response. These include a plastic yield-line analysis based on a failure pattern repeatedly observed during blast tests. In recent research it was demonstrated that yield lines can develop in fractured laminated glass through the composite bending action of the glass fragments, working in compression, together with the interlayer working in tension. This paper investigates the influence of the inertia loading associated with blast response, which has not been explicitly studied previously, with the aim of understanding the pattern of yield lines observed in blast tests. Impact tests are performed on laminated glass specimens using foam projectiles launched from a gas gun, which simulate the loading from a blast pulse. These tests demonstrate that the yield line pattern formed under short-duration dynamic loading depends on the loading intensity, thereby providing further evidence of a dynamic, plastic collapse mechanism in which inertia plays a significant role.

1. Introduction

During an external blast event, such as a terrorist attack or an accidental explosion, the façade of a building must act as the first barrier of defence to the building occupants. Failure of the façade results in the blast wave penetrating the building interior, which may then cause further damage or injuries. Laminated glass panels are increasingly used in façades to enhance the blast resilience of buildings. They are essentially composite glass-polymer sandwich structures, typically comprising of two glass plies with a polymer interlayer. The most common interlayer used in laminated glass for building façades is polyvinyl butyral (PVB).

The blast response of PVB-laminated glass panels, and particularly the post-fracture response, when all glass plies have fractured, is a complex multiscale, multi-physics problem that is still not well understood. Various researchers have studied this problem by means of full-scale blast tests using high explosive detonations and shock-tube simulations. These tests typically focus on recording the global peak-displacement time-history of a panel through all stages of deformation (i.e., pre- and post-fracture), with some researchers also presenting images of the failed panel [1–4]. Fig. 1(a), (b) and (c) show some examples of the consistent fracture pattern observed in these tests: a doubly-symmetric pattern in which the fracture and crushing of the glass is concentrated along lines of high strain, which resemble a central rectangle connected by four diagonals to the corners of the panel.

Most existing blast analysis methods do not account for this fractured pattern. They typically rely on finite-element and equivalent-single-degree-of-freedom models that assume a pure membrane response of the interlayer to describe the post-fracture stage of the panel (see Angelides & Talbot [5], for a review of existing analysis methods). Yuan et al. [6] and Del Linz et al. [7] were the first researchers to develop analytical models for the post-fracture stage and to account for the observed fracture pattern. In these analytical models, a yield line pattern is adopted for deriving the mid-panel displacement time-history of the fractured panel, assuming that membrane strains accumulate only at the yield line locations (see Angelides & Talbot [5], for a comparison of the two models). However, no justification for the formation of yield lines is provided and the pattern is simply adopted by reference to the

* Corresponding author.
E-mail address: s.angelides@steel-sci.com (S.C. Angelides).
[1] Present address: Steel Construction Institute, Silwood Park Campus, Ascot, SL5 7QN, UK.

https://doi.org/10.1016/j.compstruct.2023.117286
Received 13 February 2023; Received in revised form 19 May 2023; Accepted 17 June 2023
Available online 20 June 2023

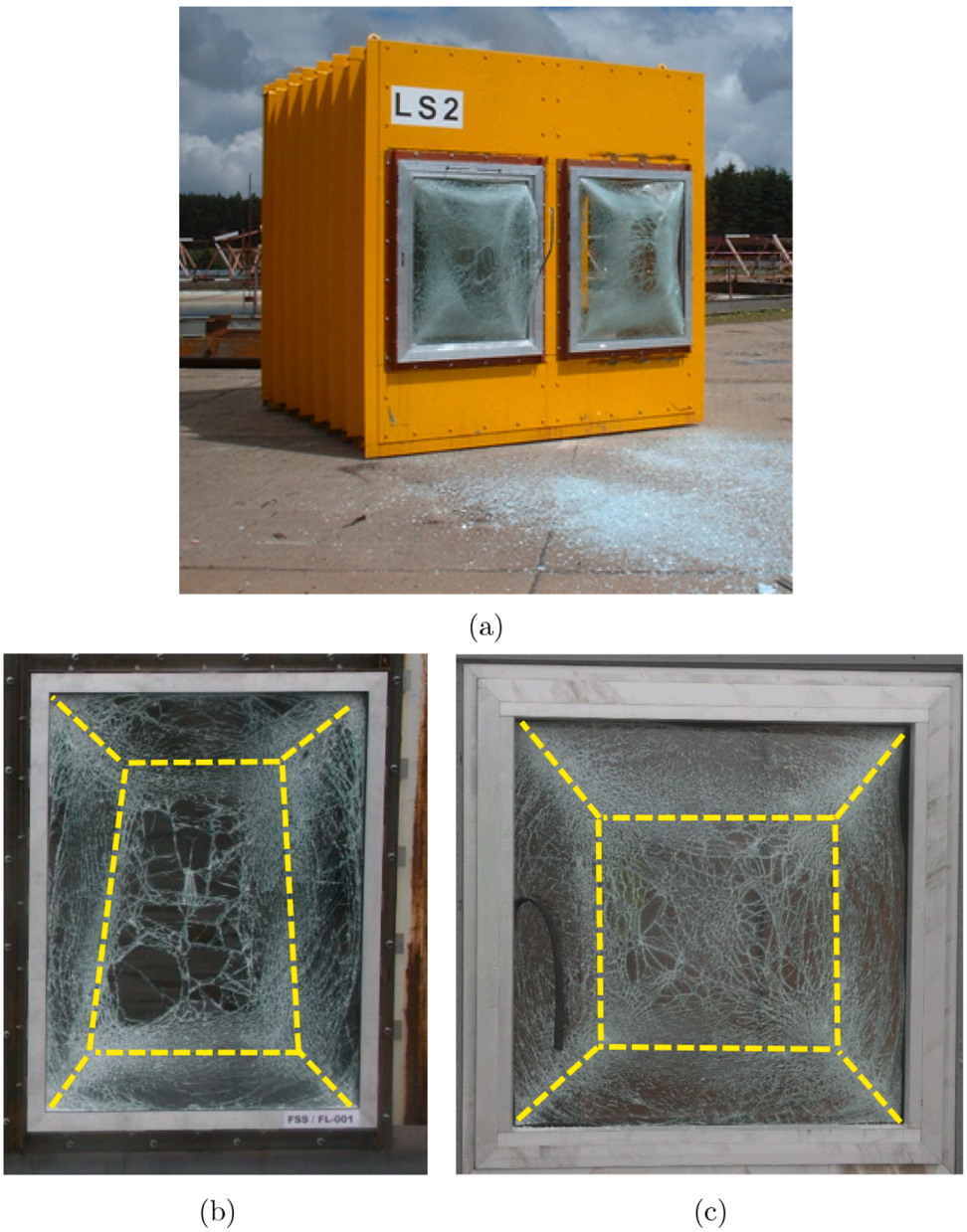

Fig. 1. The consistent fracture pattern of laminated glass panels observed in full-scale blast tests (courtesy of D.J. Goode and Associates Ltd): (a) Typical blast chamber used for the testing of laminated glass panels, (b) and (c) the yield lines formed are highlighted with yellow dashed lines.

experimental observations. Although this is not explicitly discussed, the formation of yield lines implies a post-fracture bending response of the panel, contradicting the pure membrane assumption considered in finite-element and equivalent-single-degree-of-freedom models.

The formation of yield lines in fractured laminated glass panels under blast loading was subsequently investigated by Angelides et al. [8] using a first-principles approach to examine the effects of high strain-rates. It was hypothesised that plastic hinges (and therefore yield lines) develop from an approximate elastic–plastic composite bending action of the glass fragments, working in compression, together with the interlayer working in tension. This was demonstrated by deriving analytical models showing that the bending capacity of the fractured panel is significantly enhanced at the high strain-rates associated with blast loading due to the visco-elastic stiffening of the PVB interlayer. These analytical models were subsequently validated experimentally with low-temperature bending tests that simulated the effect of high strain-rates with low temperatures [9–10]. In these experiments, static collapse loads – that is, the quasi-static loads at which a collapse mechanism forms – were derived for three different cross-sections of simply-supported specimen (Table 1). It was found that the collapse loads of the low-temperature specimens were enhanced by two orders of magnitude, compared to those at room temperature, which, given the observed time–temperature dependency of PVB, is expected to translate to a similar enhancement at the high strain-rates associated with typical blast loading.

The work described above focused solely on the effects of high strain-rates, assuming quasi-static loading that ignores the effects of inertia. For impulsive loads, of high intensity and short-duration, such as blast loading, inertia can provide significant resistance, preventing excessive deformation of a panel even for loads greater than the static collapse load.

For a simply-supported ductile beam, with a uniformly distributed load F_A, a quasi-static collapse mechanism with a single plastic hinge forming at mid-span is anticipated once the magnitude of the force exceeds the static collapse load (F_C), as shown in Fig. 2(a). In this context, ductility refers to beams that can be idealised as elastic-perfectly plastic

Table 1
Ultimate static loading capacities of pre-fractured laminated glass specimens, averaged from recorded room- and low-temperature three-point bending tests [9]. Room temperature tests were performed only for the CS1 specimens.

Specimen details		Static collapse load, F_C [N]	
Designation	**Laminate Thickness**	**Room Temperature (low strain-rates)**	**Low Temperature (high strain-rates)**
CS1	$h_G = 3$ mm / $h_{PVB} = 0.38$ mm / $h_G = 3$ mm	2.28	236
CS2	$h_G = 3$ mm / $h_{PVB} = 1.52$ mm / $h_G = 3$ mm	N/A	734
CS3	$h_G = 6$ mm / $h_{PVB} = 1.52$ mm / $h_G = 6$ mm	N/A	1,567

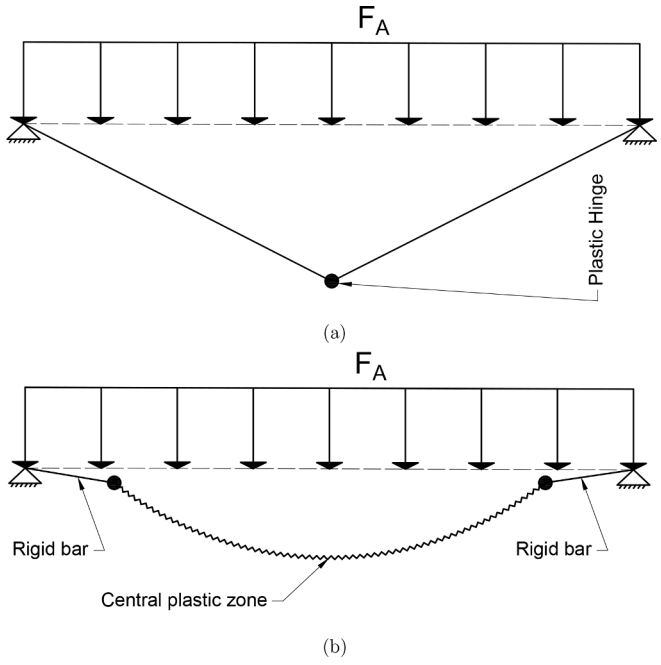

Fig. 2. The collapse mechanism (in elevation) of a simply-supported ductile beam under a short-duration pulse load applied uniformly along the span: (a) quasi-static to moderate dynamic loading ($F_A \leq 3F_C$) and (b) intense dynamic loading ($F_A > 3F_C$).

materials. For moderate dynamic loads ($F_A \leq 3F_C$), in which the force is applied as a short-duration pulse (i.e., relative to the fundamental natural period), the same collapse mechanism occurs. However, for intense dynamic loads ($F_A > 3F_C$), the same quasi-static collapse mechanism would violate plasticity, as the internal bending moment would exceed the plastic moment capacity, as demonstrated by Stronge and Yu [11] for a cantilever beam. Consequently, the mechanism switches to one of travelling hinges, with the initial form shown in Fig. 2(b), comprising a central plastic zone formed between two rigid bars [12]. Similar behaviour is observed in ductile plates under uniform pressure loading. Yu and Chen [13] concluded that the switch from moderate to intense pressure loading for two-way spanning, fully-simply-supported rectangular plates occurs at between two and three times the static collapse load and depends on the aspect ratio of the plate. The resulting collapse mechanisms are shown in Fig. 3(a) and (b). The mechanism under intense loading resembles the pattern observed in laminated glass panels under blast loading, shown in Fig. 1.

This paper aims to contribute to our understanding of the blast response of laminated glass by investigating if the failure pattern consistently observed during full-scale blast tests is the consequence of inertia under intense short-duration pulses. Demonstrating this would provide a first-principles understanding of the yield line pattern adopted empirically in existing analytical models (i.e., [6–7]). To examine the collapse mechanisms forming under pulse loading, dynamic bending tests are performed on PVB-laminated glass beam specimens. This is achieved by launching foam projectiles from a gas-gun at high velocity and impacting the specimens at mid-span, thereby applying a patch load. Martin and Symmonds [14] demonstrated that similar collapse mechanisms to those forming under uniform loading (Fig. 2) also occur under patch loading. The change in the load type results in discontinuities in the acceleration diagram along the length of the beam that

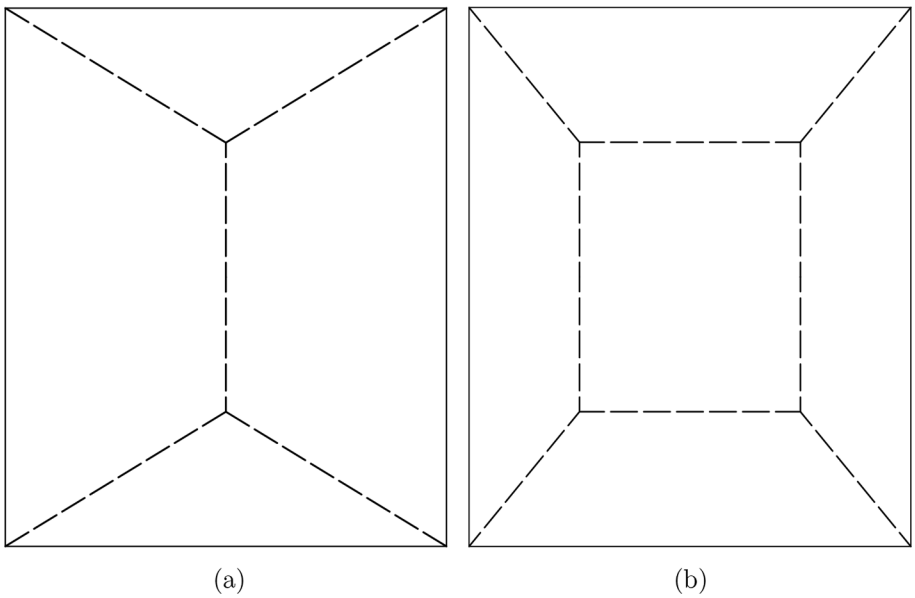

Fig. 3. The collapse mechanism (in plan) of a fully-simply-supported ductile rectangular plate under a short-duration uniform pressure pulse: (a) quasi-static to moderate dynamic pressure loading and (b) intense dynamic pressure loading.

require laborious numerical integrations to obtain a complete solution. Nevertheless, these small-scale tests are suitable for examining in detail the initial collapse mechanisms forming in laminated glass specimens via a systematic and controlled series of tests, and they are significantly cheaper than the conventional full-scale high-explosive detonation tests. The experimental work, performed on both intact and pre-fractured specimens on pinned supports, with and without axial restraints, is first described. This is followed by the results and a discussion of the influence of inertia and axial restraint on the response.

2. Experimental method

In gas-gun impact tests, short-duration pressure pulses are generated by impacting a target with foam projectiles launched from a gas-gun at high velocity (Fig. 4a). Radford et al. [15] defined the characteristics of the pulse resulting from aluminium foam projectiles by impacting an instrumented Kolsky pressure bar. Such projectiles typically generate pulses with peak pressures of the order of 10 to 300 MPa, and have therefore been used to simulate underwater shock loading [16–22]. With air-blast loading, such high pressures are only relevant for structures located very close to the explosive (i.e., reflected pressures in the near-field with scaled distances ranging from 0.78 to 0.12 m/kg$^{1/3}$ for free-air charges) [23]. Such cases are rare, as physical barriers are often installed in front of buildings that are considered at risk from a terrorist attack, to prevent potential vehicle bombs from approaching the façade. Consequently, softer projectiles that generate lower peak pressures are required for investigating the blast response of laminated glass.

Chen et al. [24] performed gas-gun impact tests with polymer foam projectiles on sandwich composite beams (carbon fibre laminated facesheets with balsa wood core), resulting in peak pressures ranging from 3.2 to 6.2 MPa. Such values are representative of reflected pressures with scaled distances ranging from 1.17 to 0.93 m/kg$^{1/3}$ for free-air charges [23]. The p_o = 3.2 MPa peak pressure is replicated in this study and corresponds to a Trinitrotoluene (TNT) charge mass of 11 kg (i.e., a large briefcase package bomb) [25] located at a range 2.6 m from the target (scaled distance = 1.17 m/kg$^{1/3}$). Due to instrumentation difficulties, an indirect, hybrid approach was used by Chen et al. [24] to measure the pressure–time history, by combining the results from impacting a dynamic force measurement bar and a dynamic piezoelectric load cell. An approximately triangular pulse was deduced, as shown in Fig. 4b, resembling the shape of the positive phase of the blast loading experienced by the front façade of a building (with respect to the explosive location) during the detonation of a high-explosive [26].

The following sections present further details of the experimental work performed for this study. A description of the experimental facilities and the glass specimens is provided, followed by a validation of the loading generated by the projectiles. Finally, an overview of the types of test performed is presented.

2.1. Experimental facilities and laminated glass specimens

The test specimens consisted of laminated glass made from two layers (or plies) of annealed soda-lime-silica glass. This type of glass is produced commercially by the float process in accordance to BS EN 572 [27]; it is readily available and is commonly used in buildings. The glass had polished edges (to minimise secondary cracking) and was laminated with a standard architectural grade PVB interlayer in a commercial, glass laminating autoclave by Phoenicia (specimens CS1) and ToughGlaze (specimens CS2 and CS3) to BS EN ISO 12543–2 [28]. The overall geometry of the specimens (total length L = 200 mm; width B = 55 mm) and the thickness of each ply was identical to the specimens previously tested by Angelides et al. [9–10] at low temperatures, as introduced in Section 1. Three different cross-sections were tested in total, with the same length and width but different thicknesses of glass and PVB, as summarised in Table 2.

The experiments were performed in the gun room laboratory of Cambridge University Engineering Department using a gas gun with a barrel diameter of 29 mm. The latter was chosen to fit projectiles with

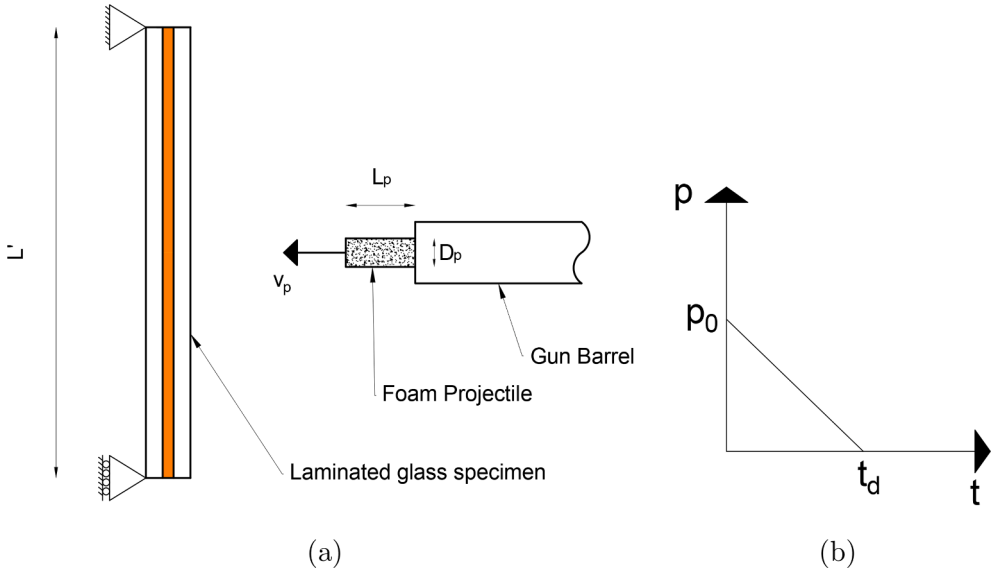

Fig. 4. (a) Diagram of a foam projectile launched from a gas gun and impacting a laminated glass specimen, and (b) the approximately triangular loading pulse resulting from gas-gun impact tests with polymer foam projectiles.

Table 2
Geometrical properties of laminated glass specimens.

Designation	Laminate Thickness	Length (*L*) [mm]	Width (*B*) [mm]
CS1	h_G = 3 mm / h_{PVB} = 0.38 mm / h_G = 3 mm	200	55
CS2	h_G = 3 mm / h_{PVB} = 1.52 mm / h_G = 3 mm	200	55
CS3	h_G = 6 mm / h_{PVB} = 1.52 mm / h_G = 6 mm	200	55

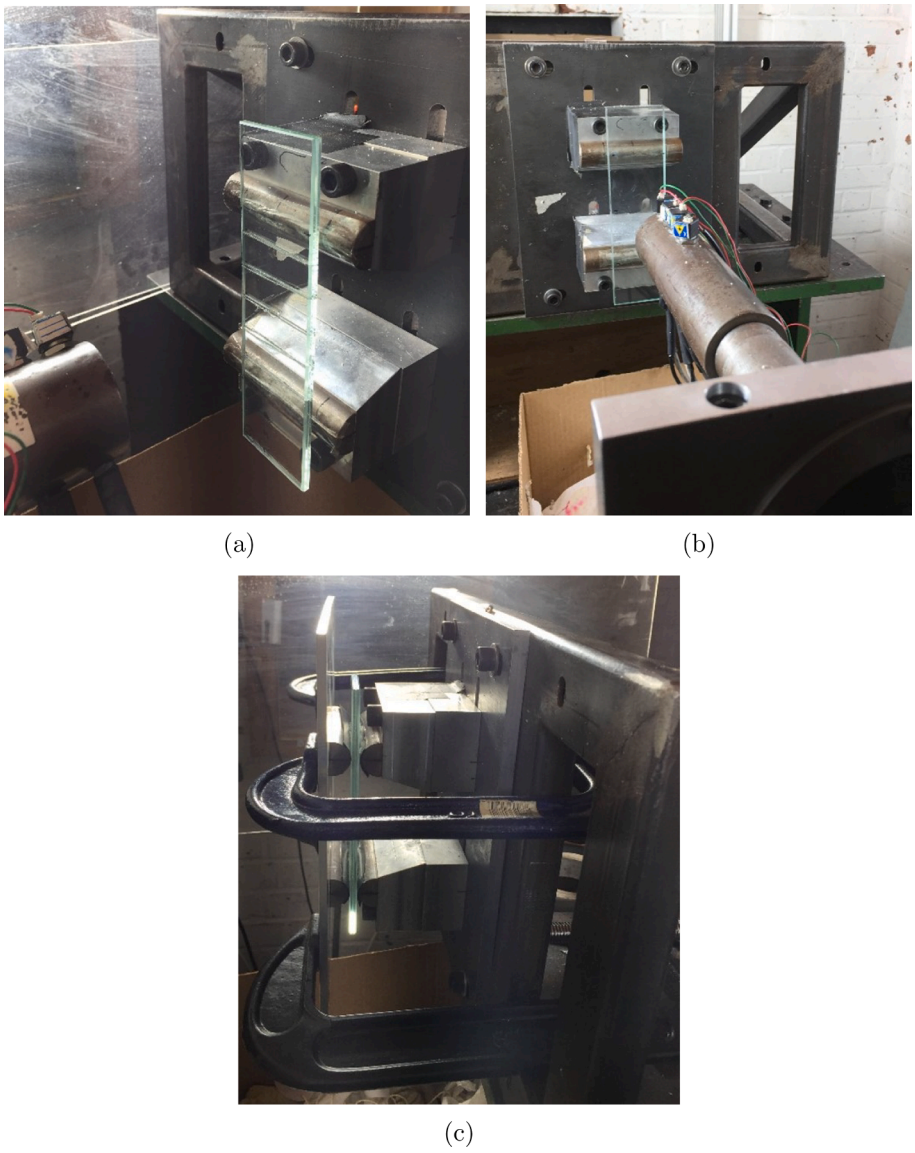

Fig. 5. Laminated glass specimens mounted on rig: (a) pre-fractured (no axial restraints), (b) intact (no axial restraints) and c) intact (with axial restraints).

diameter of $D_p = 28$ mm. For the chosen peak pressure of the pulse, $p_o = 3.2$ MPa, this achieved a peak loading of $F_A\,(t=0) = \pi\,(\frac{Dp}{2})^2\,p_o = 1{,}970$ N, which is greater than the static collapse load (F_C) for all three cross-section sizes (Table 1). The manufacturing process used by Chen et al. [24] was followed for the projectiles, using a polymer foam of density 80 kg/m^3 [29]. The diameter was found to vary across the projectiles due to manufacturing inconsistencies, most notably the layers of grease applied to the mould and the sanding of the projectiles to fit in the barrel. A lower bound value of $D_p = 25$ mm was measured, for which the peak load of $F_A = 1{,}571$ N is still greater than the ultimate static loading capacity of the glass specimens. To replicate the loading pulse recorded by Chen et al. [24], the projectiles were launched with a target velocity of $v_p = 38.1$ m/s, which was confirmed for each projectile using both laser diode velocity gates and a high-speed camera (Phantom V1610).

A rig with pinned supports was used to assess the pure bending response of the specimens (Fig. 5a and 5b). The deformation profiles and the mid-span displacement time-histories were also recorded with the high-speed camera. This rig was subsequently modified to assess the contribution of the membrane forces that are generated at large deflections: an additional plate was introduced that clamped the specimens between pinned supports, thereby generating friction that prevents axial movement, as shown in Fig. 5c.

Both pre-fractured and intact laminated glass specimens were tested, as shown in Fig. 5a and b. The former ensures that a controlled and repeatable fracture pattern is achieved by first scoring both glass plies with a diamond-tip glass cutter and then imparting a controlled impact through a bespoke jig in order to produce full-thickness cracks in both glass plies [29]. The pre-cracked pattern considered here is idealised as a series of cracks at a uniform spacing of 20 mm to allow direct comparison between tests and elicit the fundamental behaviour, although it is challenging to produce identical patterns and small variations existed between specimens. This is the same idealised pattern considered in the low temperature bending tests presented by Angelides et al. [9], and represents a lower bound solution for the post-fractured bending moment capacity of the real irregular fracture pattern formed under blast loading [10].

(a) (b) (c)

Fig. 6. Quasi-static compression tests performed on polymer foam projectiles: (a) undeformed (b) initial deformation and (c) final deformation. The clear plastic tube prevents buckling of the projectiles.

2.2. Validation of pressure time-history generated by the projectiles

Due to difficulties in recording directly the pressure time-history generated by the polymer projectiles (see Chen et al. [24]) an indirect method of validation is also adopted in this study. Two validation tests were performed to ensure that the loading generated by the manufactured projectiles results in the pulse shown in Fig. 4b, with a peak pressure of $p_o = 3.2$ MPa. First, quasi-static compression tests were performed on three foam projectiles, as shown in Fig. 6, to characterise the stress–strain response and compare it with that recorded by Chen et al. [24] at a strain-rate of 0.1 s^{-1} (Fig. 7). The recorded responses for all three projectiles agree well with those from Chen et al [24].

Following the validation of the quasi-static properties, aluminium beam specimens were impacted by the same design of projectile launched from the gas gun at a velocity of $v_p = 38.1$ m/s (the measured velocity varied from $v_p = 37.4$ to 38.1 m/s in the three tests performed). This test aimed to validate indirectly the pressure time-history generated by the projectiles, by recording the displacement time-history of the aluminium specimens with the high-speed camera and comparing it to a theoretical prediction. The mid-span displacement time-history was predicted both analytically, via modal analysis, and numerically, using the commercial FEA package RFEM Dlubal. In the former, the projectile impact pressure was converted into an equivalent point load applied at mid-span, $F_A(t) = \pi \left(\frac{D_p}{2}\right)^2 \mathrm{p(t)}$, where $p(t)$ is the pressure–time history generated by the projectile and D_p is the projectile diameter. In the latter, the aluminium specimens were modelled with 2D quadrilateral plate elements and the projectile impact was applied as a normal pressure over a circular patch. Two different projectile diameters were considered in both analyses, representing the lower ($D_p = 25$ mm) and upper ($D_p = 28$ mm) bound values of those tested, as discussed in Section 2.1.

The deformation of the aluminium specimens at various time stamps is shown in Fig. 8. An elastic deformation is observed, with the specimen

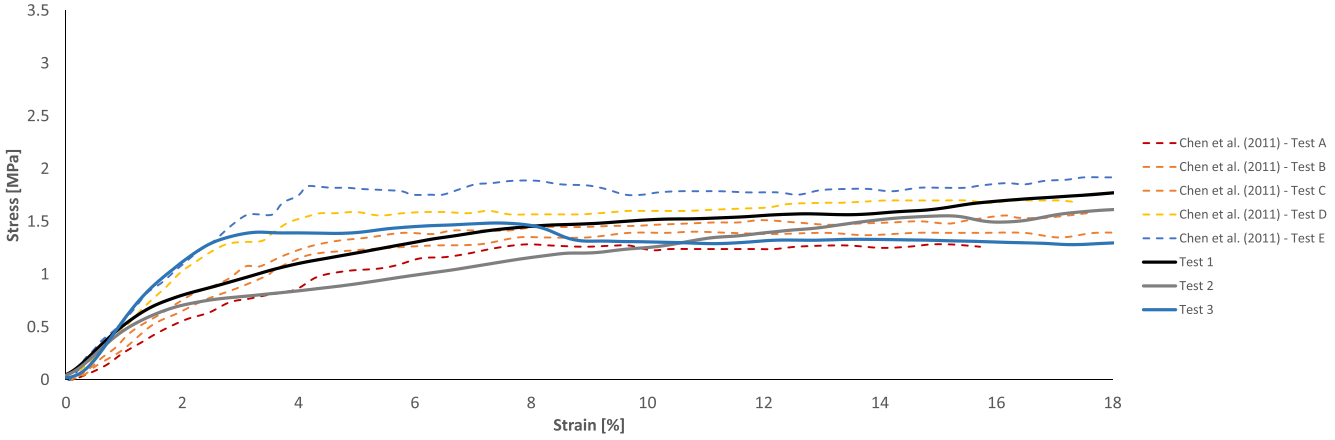

Fig. 7. Comparison of the stress–strain responses of three polymer foam projectiles recorded during quasi-static compression tests (Tests 1–3) with those (Tests A-E) digitised from Fig. 18 (density 80 kg / m^3) of Chen et al. (2011).

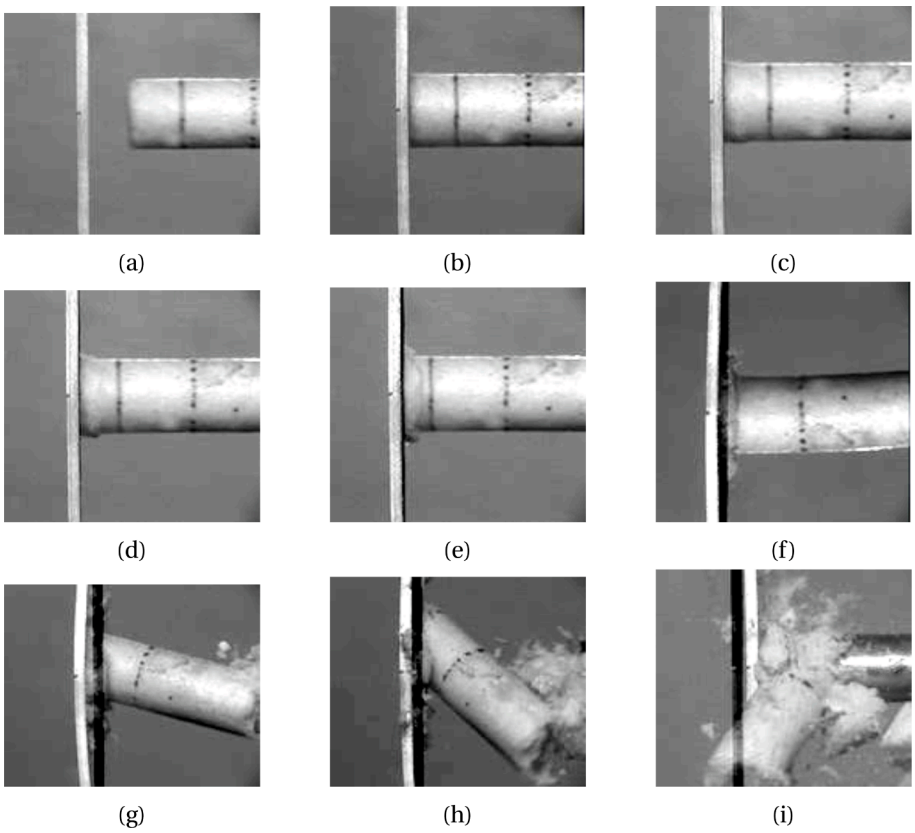

Fig. 8. Deformation of an aluminium specimen (in elevation) at different time stamps during impact with a polymer projectile: (a) projectile arriving at target, (b) t = 0 μsec, (c) 62.5 μsec, (d) t = 125 μsec, (e) t = 312.5 μsec, (f) t = 687.5 μsec, (g) t = 1437.5 μsec, (h) t = 2062.5 μsec and (i) t = 3187.5 μsec. The initial undeformed state of the aluminium specimen is visible as a black shadow.

rebounding. The instant the projectile impacts the specimen is labelled as t = 0 μsec (Fig. 8b), with the camera subsequently recording frames every 62.5 μsec. The projectile crushing is initiated at the tip of the projectile (Fig. 8c to f). At larger deflections of the specimen, the projectile remains intact and starts to rotate, eventually resulting in a shear failure of the projectile (Fig. 8g). This shear failure, which was observed in all three tests, did not interfere with the inbound response stage of the specimen. This is demonstrated by the recorded displacement time-history for all three tests shown in Fig. 9, which agrees with the theoretical predictions. For all three tests, the recorded displacements fall within the upper (D_p = 28 mm) and lower (D_p = 25 mm) bound predictions. It is noted that the projectile interferes with the response during the rebound stage (Fig. 8h to i). This is also observed in Fig. 9, as discrepancies are noticed between the experimental and theoretical predictions during the rebound stage. It is therefore concluded that the polymer projectiles provide the anticipated impulse for the experimental

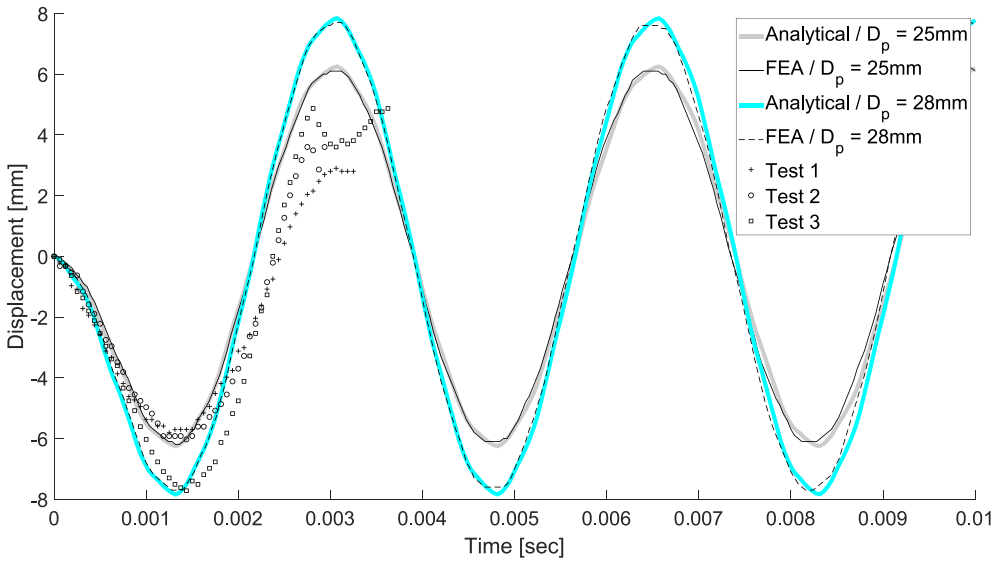

Fig. 9. Comparison of theoretical predictions (analytical and FEA) with the experimentally recorded (Tests 1–3) mid-span displacement time-history of aluminium specimens impacted by foam projectiles.

investigation of the inbound response of the laminated glass specimens.

2.3. Overview of tests performed

The performance of laminated glass under short-duration pulse loading was assessed through nine different types of impact test (type A-I), as summarised in Table 3. Each type was repeated three times to obtain confidence in the experimental results, thereby amounting to 27 tests in total. Three independent variables were considered, namely: boundary conditions (pinned supports with or without axial restraint); the pre-fractured state of the specimens (uniform pre-fractured pattern or intact specimens) and the specimen cross-section size (CS1, CS2 and CS3).

A constant span of $L' = 11$ cm was chosen for all the test types. This is identical to the span considered in the low temperature quasi-static bending tests of Angelides et al. [9], thereby enabling a direct assessment of the effects of inertia experienced by the specimens under the dynamic loading.

Table 3
Overview of impact tests performed on laminated glass specimens.

Test Type	Boundary conditions	Specimens pre-fractured	Specimen cross-section
A	No axial restraint	Yes	CS1
B	No axial restraint	Yes	CS2
C	No axial restraint	Yes	CS3
D	No axial restraint	No	CS1
E	No axial restraint	No	CS2
F	No axial restraint	No	CS3
G	Axial restraint	No	CS1
H	Axial restraint	Yes	CS1
I	Axial restraint	Yes	CS3

3. Results

The experimental results are categorised based on the boundary conditions, i.e., without axial restraint (test type A-F) and with axial restraint (test type G-I).

3.1. Impact tests without axial restraint (type A-F)

The recorded projectile velocity ranged from $v_p = 34.2$ m/s to 43.4 m/s. The deformation of the three pre-fractured cross-sections (CS1-3) is illustrated in Figs. 10 to 12, which show photographs at various time stamps from representative tests of each of the three sizes. All three CS1 specimens tested resulted in PVB tearing failure at large deflections. In contrast, PVB tearing was not observed in any of the CS2 and CS3 tests. The recorded mid-span displacement time-history of all three test types is presented in Fig. 13. The results show a relatively good consistency across the three, nominally identical, tests for all cross-section sizes. The small deviations are attributed to the inherent variability in the material properties and the challenge of producing identical pre-fracture patterns, as noted in Section 2.1. A stiffer response is consistently observed for the thicker specimens.

The deformation of the three intact cross-sections (CS1-3) is shown in Figs. 14 to 16. All the CS1 and CS2 intact specimens fractured during the tests. The glass ply on the far face of the specimen, not in contact with the projectile, was the first to fracture in all specimens, consistent with the state of stress expected from the bending action. Following the fracture of this ply (Fig. 15d), the second ply fractured almost instantaneously (Fig. 15e), i.e., within the 62.5 μsec to the next camera frame. This was followed by PVB tearing failure in all three intact CS1 specimens, in a similar manner to the response observed for the pre-fractured specimens. In contrast, all three CS3 specimens remained intact during the impact tests.

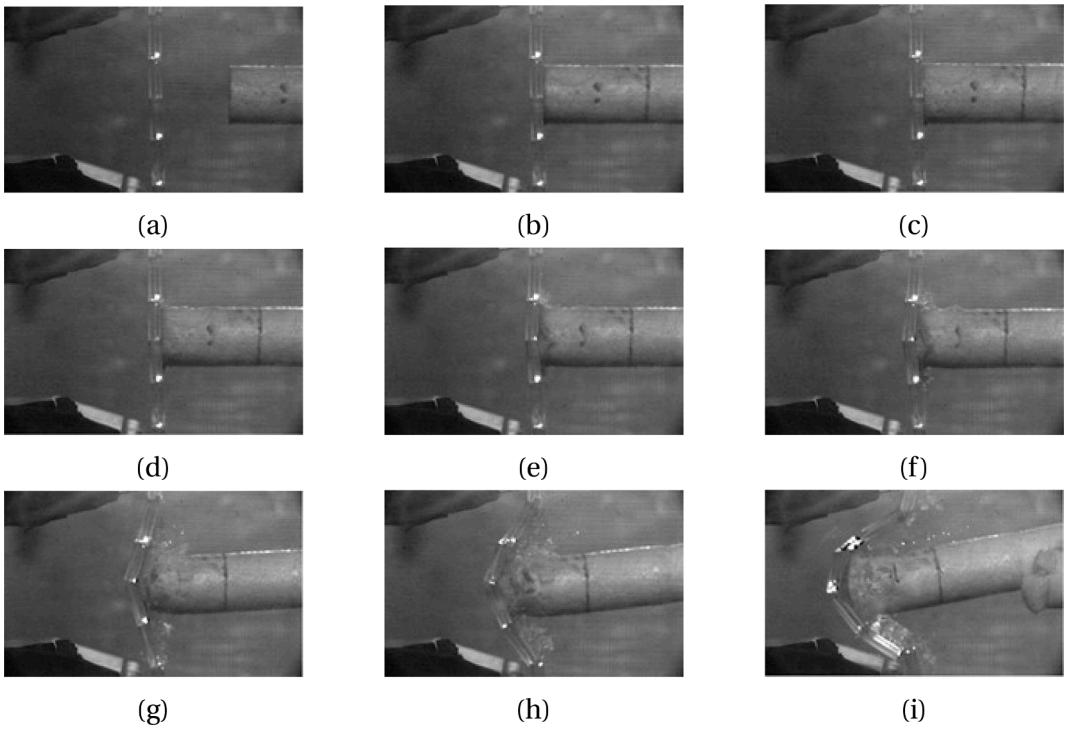

Fig. 10. Deformation of a pre-fractured CS1 laminated glass specimen (test type A, in elevation) at different time stamps during impact with a polymer projectile: (a) projectile arriving at target, (b) t = 0 μsec, (c) 62.5 μsec, (d) t = 125 μsec, (e) t = 375 μsec, (f) t = 500 μsec, (g) t = 937.5 μsec, (h) t = 1437.5 μsec and (i) t = 2312.5 μsec.

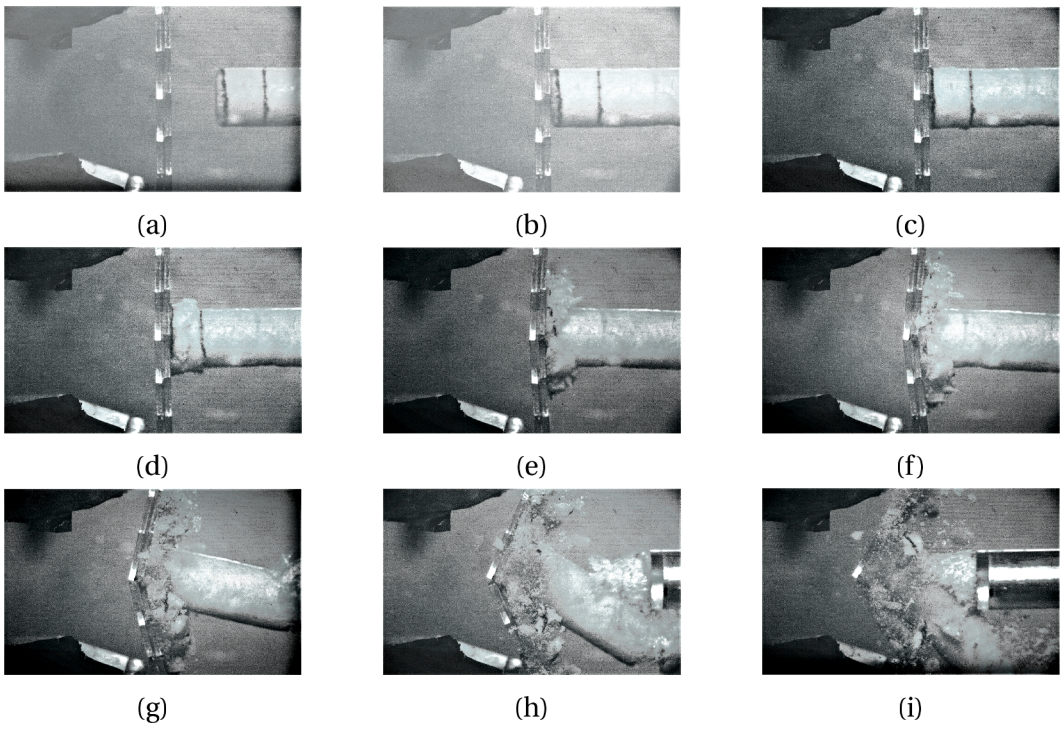

Fig. 11. Deformation of a pre-fractured CS2 laminated glass specimen (test type B, in elevation) at different time stamps during impact with a polymer projectile: (a) projectile arriving at target, (b) t = 0 μsec, (c) 125 μsec, (d) t = 312.5 μsec, (e) t = 812.50 μsec, (f) t = 1125 μsec, (g) t = 1812.5 μsec, (h) t = 2750 μsec and (i) t = 3562.5 μsec.

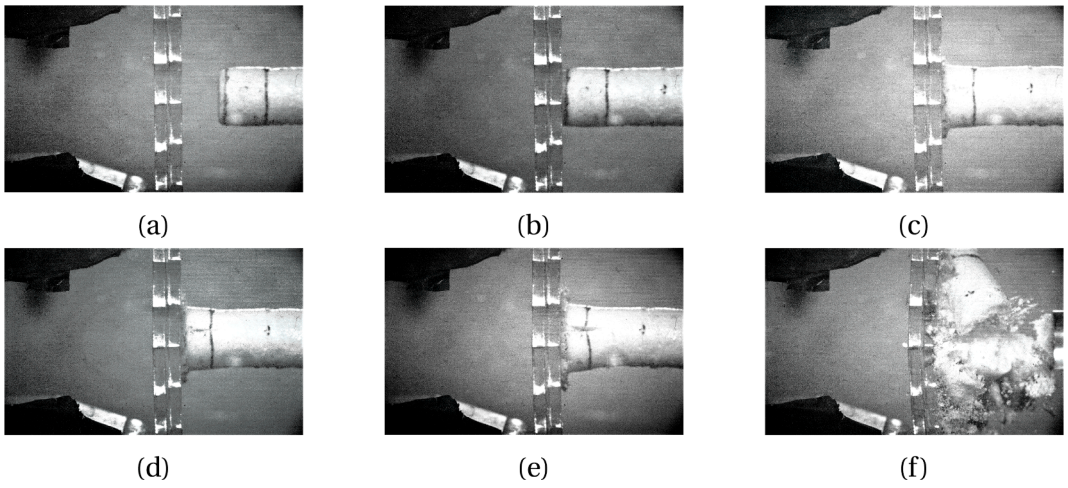

Fig. 12. Deformation of a pre-fractured CS3 laminated glass specimen (test type C, in elevation) at different time stamps during impact with a polymer projectile: (a) projectile arriving at target, (b) t = 0 μsec, (c) 312.5 μsec, (d) t = 375 μsec, (e) t = 562.5 μsec and (f) t = 2562.5 μsec.

3.2. Impact tests with axial restraint (type G-I)

The recorded projectile velocity ranged from v_p = 36.9 m/s to 41.3 m/s. The deformation of the two pre-fractured cross-sections (CS1 and CS3) is illustrated in Figs. 17 and 18. PVB tearing at large displacements was observed for all three pre-fractured CS1 specimens tested. After tearing of the PVB, the end portions of the specimen remained attached to the supports due to the introduction of the axial restraints, as shown in Fig. 19. In contrast, smaller displacements and no PVB tearing were observed for the thicker pre-fractured CS3 specimens. A comparison of the mid-span displacement time-histories for the pre-fractured CS1 and CS3 specimens with and without axial restraint is presented in Fig. 20a and 21b.

The deformation of an intact, axially restrained CS1 specimen is shown in Fig. 21. All three CS1 specimens tested with axial restraint remained intact during impact. For this reason, it was decided not to proceed with tests of intact, axially restrained specimens of the thicker cross-sections CS2 and CS3.

4. Discussion

The deformation patterns observed for the three cross-section sizes, for both intact and pre-fractured specimens, are first evaluated, followed by a discussion of the effects of axial restraint.

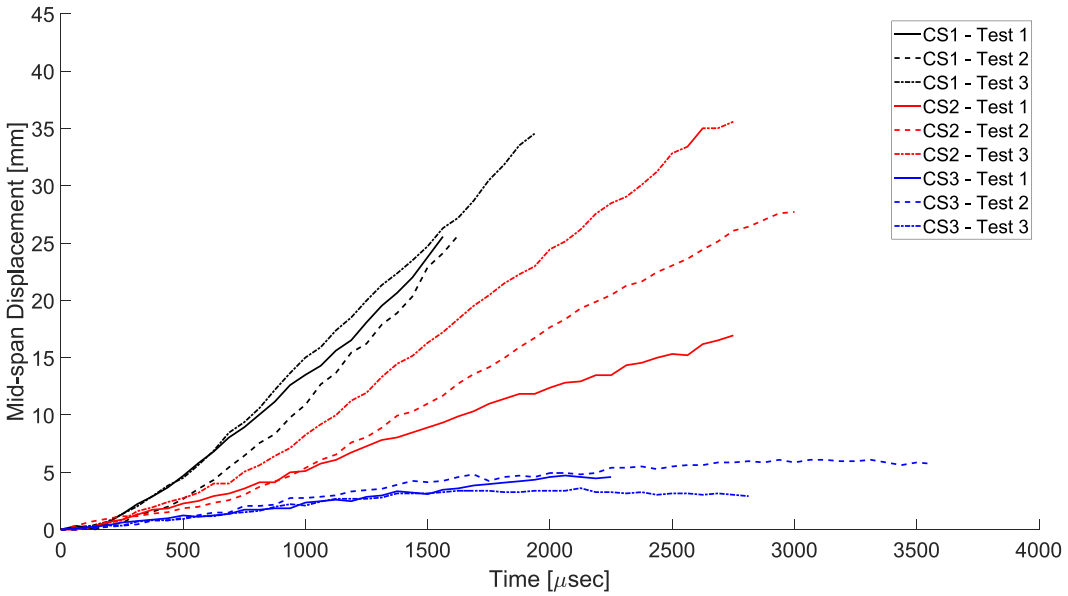

Fig. 13. Mid-span displacement time-histories of pre-fractured laminated glass specimens of three cross-section sizes CS1 (test type A), CS2 (test type B) and CS3 (test type C) recorded during impacts with polymer projectiles.

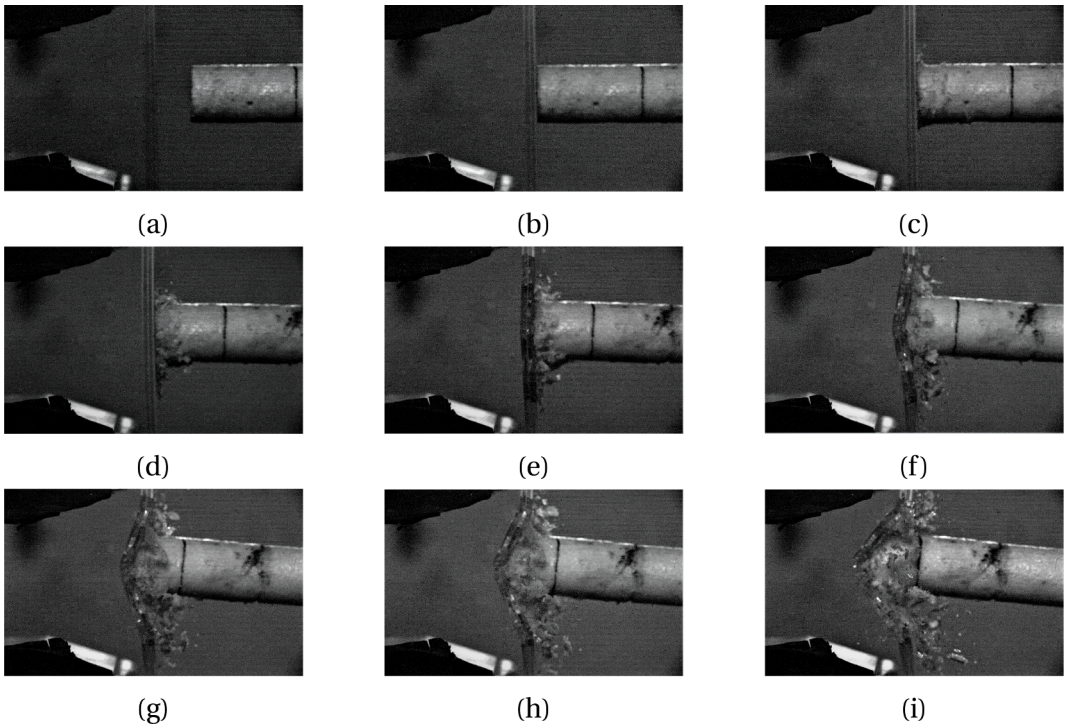

Fig. 14. Deformation of an intact CS1 laminated glass specimen (test type D, in elevation) at different time stamps during impact with a polymer projectile: (a) projectile arriving at target, (b) t = 0 μsec, (c) 250 μsec, (d) t = 687.5 μsec, (e) t = 875 μsec, (f) t = 1187.5 μsec, (g) t = 1437.5 μsec, (h) t = 1562.5 μsec and (i) t = 1937.5 μsec.

4.1. Deformation patterns under intense and moderate dynamic loading

Two distinct collapse mechanisms were observed in the impact tests of the specimens. The first consists of a single plastic hinge at mid-span, with the specimen behaving as two rigid bars on either side. This was observed consistently for the pre-fractured CS2 (test type B) and CS3 (test type C) specimens and for the intact CS2 specimens (test type E), as shown in Fig. 22b, c and d, respectively. In contrast, the mechanism observed for the pre-fractured and intact CS1 specimens (test types A and D) involved the formation of two further plastic hinges located closer to the supports, as highlighted in Fig. 23b and c. The same collapse mechanism was also observed in the axially restrained pre-fractured CS1 specimens (test type H), as shown in Fig. 23d. The axially restrained intact CS1 (test type G), the intact CS3 (test type C) and the axially restrained pre-fractured CS3 (test type H) specimens did not collapse during the tests. With the former two, the specimens remained unfractured, and with the latter, the specimen displacements were very small.

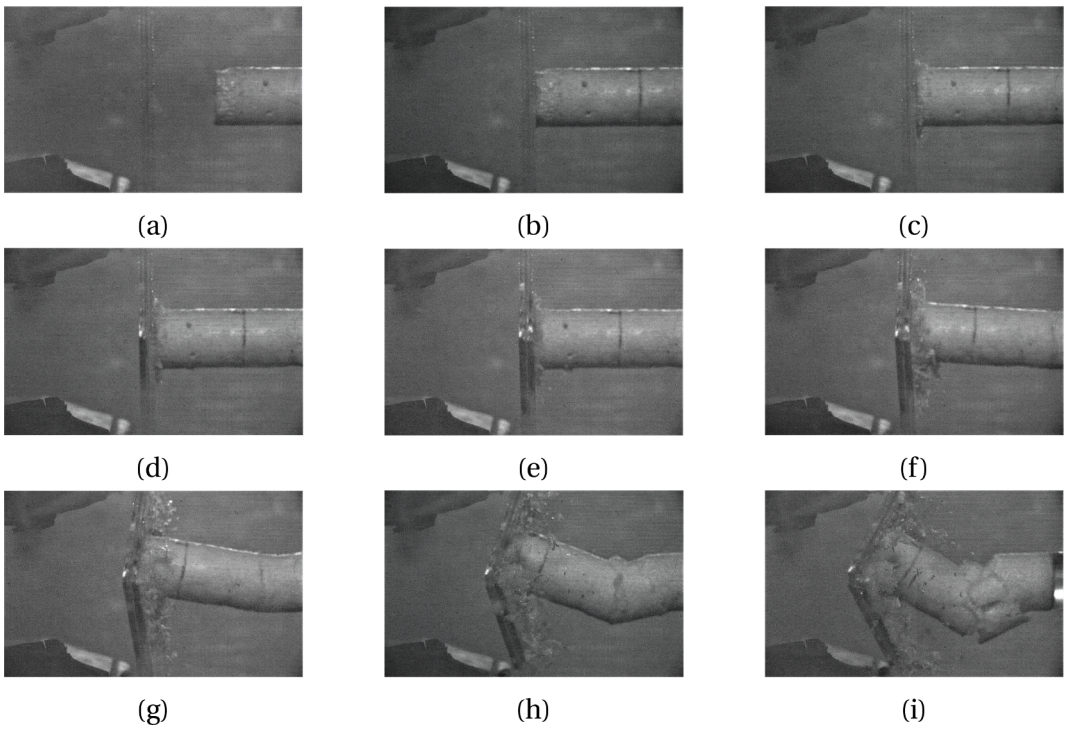

Fig. 15. Deformation of an intact CS2 laminated glass specimen (test type E, in elevation) at different time stamps during impact with a polymer projectile: (a) projectile arriving at target, (b) t = 0 μsec, (c) 250 μsec, (d) t = 312.5 μsec, (e) t = 375 μsec, (f) t = 750 μsec, (g) t = 1250 μsec, (h) t = 1812.5 μsec and (i) t = 2312.5 μsec.

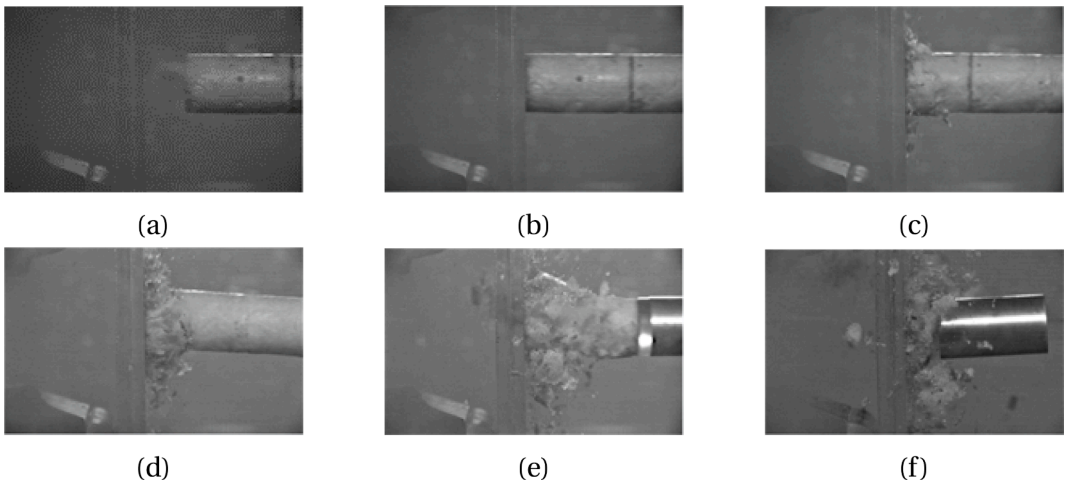

Fig. 16. Deformation of an intact CS3 laminated glass specimen (test type F, in elevation) at different time stamps during impact with a polymer projectile: (a) projectile arriving at target, (b) t = 0 μsec, (c) 687.5 μsec, (d) t = 1375 μsec, (e) t = 2687.5 μsec and (f) t = 4500 μsec.

The first of the two collapse mechanisms observed (Fig. 22a) occurs under the application of quasi-static, uniformly distributed or patch loads to simply-supported ductile beams. The plastic hinge forms at mid-span, as this is the location with the highest internal bending moment, and leads directly to collapse for these statically determinate structures. The same mechanism also occurs under the application of short-duration pulses of moderate intensity, defined as pulses with peak pressures less than three times the static collapse load, as discussed in Section 1. The pre-fractured CS2 and CS3 specimens fall into this category, as the peak loading generated by the projectiles (ranging from F_A = 1,571 N to 1,970 N) is less than three times the static collapse load of the CS2 (F_C = 3 × 734 = 2,202 N) and CS3 (F_C = 3 × 1,567 = 4,701 N) specimens (see Table 1). The same applies for the intact CS2 specimens, as the static collapse load of these specimens, which have a random fracture pattern generated during impact, is expected to be greater than the capacity of the specimens with the idealised uniform pattern [10].

The second collapse mechanism observed (Fig. 23a) is known to occur under the application of short-duration pulses of high intensity, defined as pulses with peak pressures greater than three times the static collapse load. The same mechanism is also observed in Fig. 23b to d, as the pre-fractured CS1 specimens fall into this category, with the peak loading (ranging from F_A = 1,571 N to 1,970 N) being greater than three times the static collapse load of the CS1 specimens (F_C = 3 × 236 = 708 N).

These observations provide further evidence of the ability of laminated glass to develop plastic hinges, and therefore yield lines, as part of

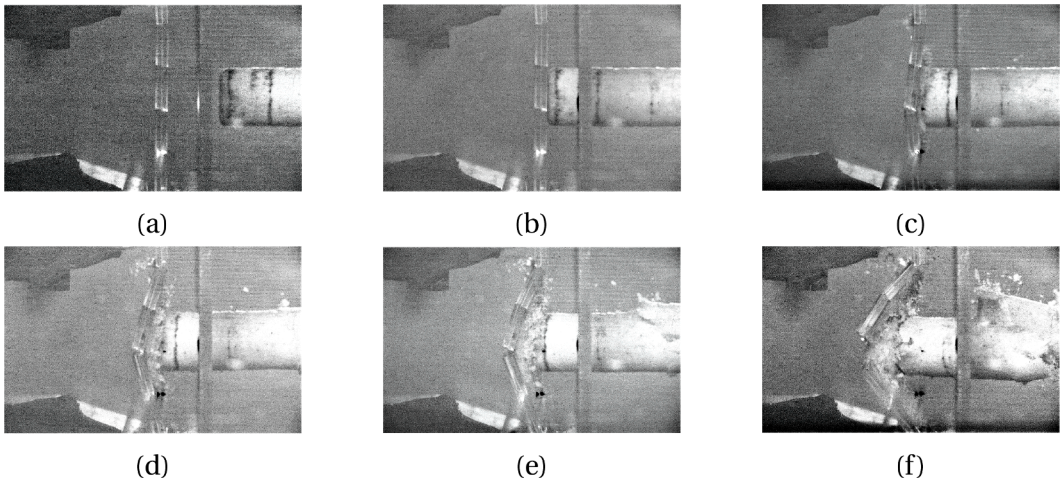

Fig. 17. Deformation of an axially restrained pre-fractured CS1 laminated glass specimen (test type H, in elevation) at different time stamps during impact with a polymer projectile: (a) projectile arriving at target, (b) t = 0 μsec, (c) 625 μsec, (d) t = 1000 μsec, (e) t = 1187.5 μsec and (f) t = 1937.5 μsec.

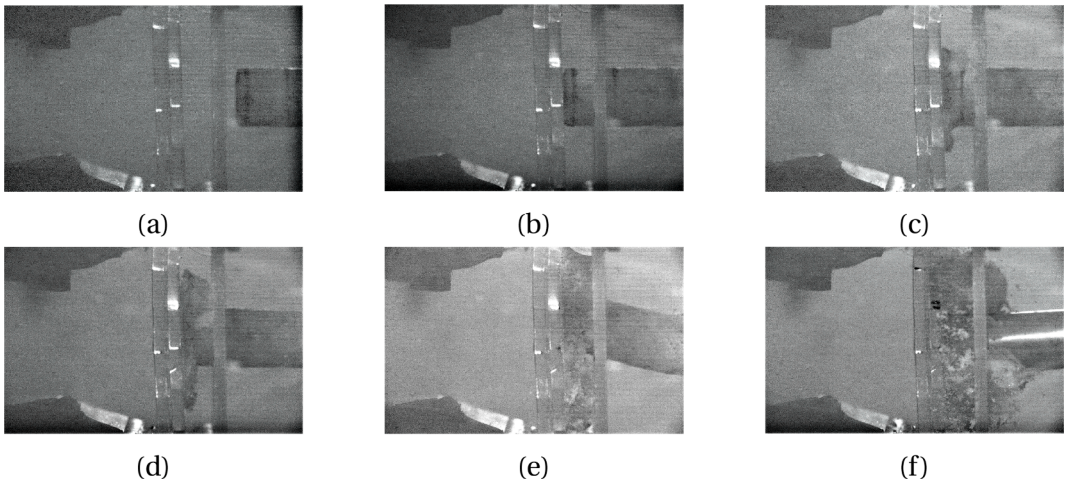

Fig. 18. Deformation of an axially restrained pre-fractured CS3 laminated glass specimen (test type I, in elevation) at different time stamps during impact with a polymer projectile: (a) projectile arriving at target, (b) t = 0 μsec, (c) 750 μsec, (d) t = 1125 μsec, (e) t = 2187.5 μsec and (f) t = 4562.5 μsec.

a plastic collapse mechanism. The observation of two distinct mechanisms, with their dependence on loading intensity, demonstrates that these are not solely a quasi-static phenomenon but rather a dynamic one in which inertia plays a significant role.

The behaviour of the of one-way spanning, simply-supported specimens, tested here under mid-span patch loading, may be extrapolated to two-way spanning plates under uniform pressure, as shown in Fig. 3a and b, with the latter forming under intense loading and resembling the failure pattern observed in blast tests (Fig. 1). This helps to provide a robust, first-principles justification for the yield line patterns adopted empirically in the analytical models of Yuan et al. [6] and Del Linz et al. [7] that were discussed in Section 1. However, further research is required to confirm if the response under intense pulses is typically described by two separate phases. Rigid-plastic structural dynamics (i.e., the theory of travelling hinges) assumes that, in the second phase, the collapse mechanism converges to that observed under moderate loading [30]. The first phase (labelled as 'transient') is observed in Fig. 23b to d, but the second phase (labelled as 'stationary') was not observed during the impact tests, as tearing failure of the PVB terminated prematurely the response of all the CS1 specimens.

4.2. Influence of axial restraint

Table 4 compares the observed failure modes of the specimens tested with and without axial restraint. These failure modes were consistently observed across the three, nominally identical, impact tests performed for each test type.

A comparison of the intact specimen response (test type D and G), highlights the effects of axial restraint on the pre-fracture stage of laminated glass. As described by the analytical models derived by Angelides et al. [8], the introduction of axial restraint results in a combined bending and membrane action that results in smaller deflections compared to simple bending (i.e., without axial restraint). In addition, the axial restraint enhances the pre-fracture load capacity, as the combined bending and membrane stresses result in lower total longitudinal stresses compared to simple bending. This was evident from the impact tests, with the axially restrained specimens resisting the loading without fracturing, compared to the unrestrained boundary condition where the specimens consistently fractured.

The influence of axial restraint on the post-fracture stage may be evaluated from the recorded mid-span displacement time-history shown in Fig. 20. An almost identical response is observed for the CS1 pre-fractured specimens with and without axial restraints (Fig. 20a). The absence of differences in this instance is attributed to the brittle failure

Fig. 19. Side view of the pinned supports providing axial restraint to a pre-fractured CS1 glass specimen (test type H) after impact with the polymer projectile.

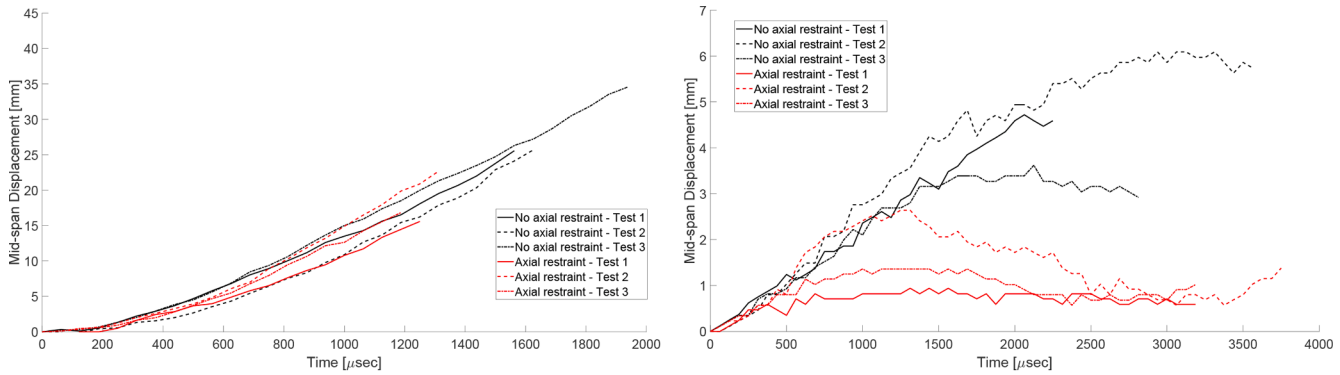

Fig. 20. Comparison of mid-span displacement time-histories of pre-fractured laminated glass specimens with and without axial restraint recorded during impacts with polymer projectiles: (a) CS1 and (b) CS3.

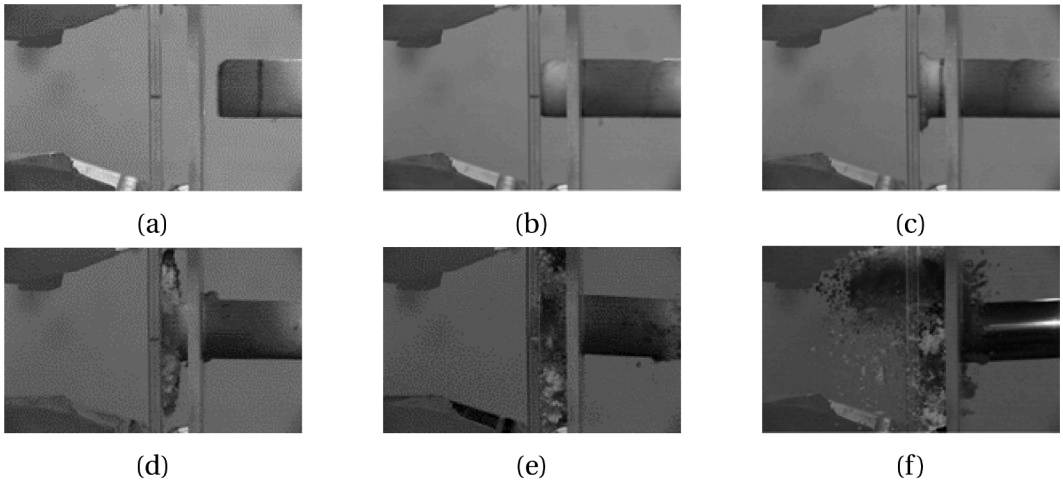

Fig. 21. Deformation of an axially restrained intact CS1 laminated glass specimen (test type G, in elevation) at different time stamps during impact with a polymer projectile: (a) projectile arriving at target, (b) t = 0 μsec, (c) t = 312.5 μsec, (d) t = 1187.5 μsec, (e) t = 2062.5 μsec and (f) t = 3937.5 μsec. The steel plate of the modified rig is also visible.

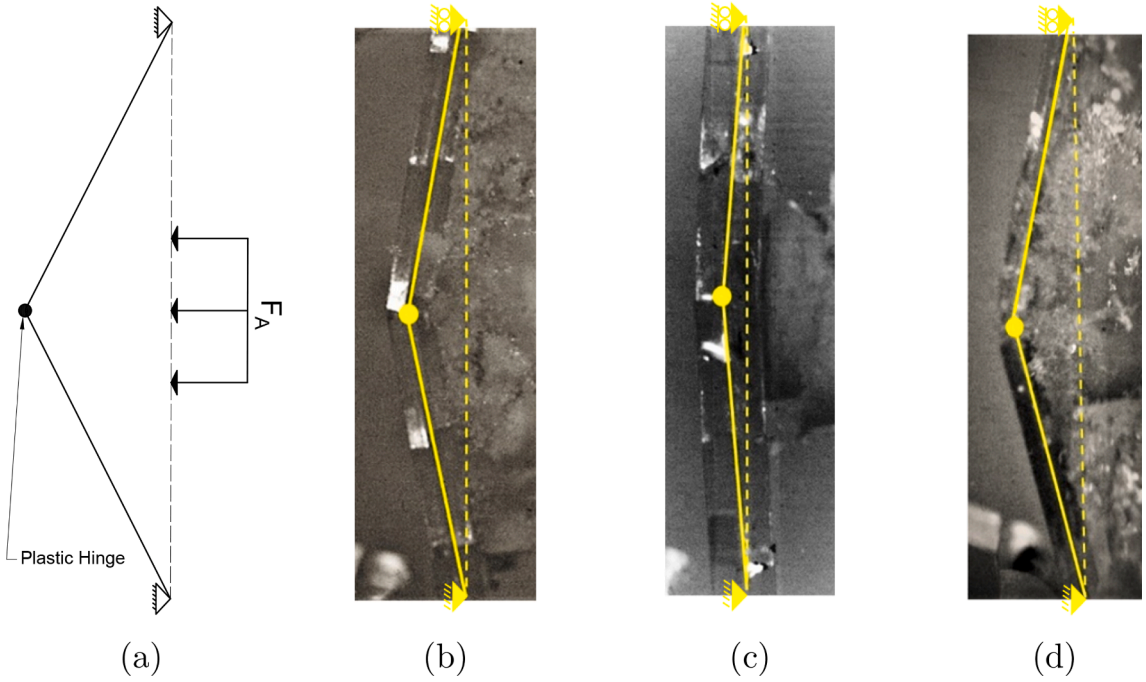

Fig. 22. Comparison of the theoretically predicted and experimentally recorded deformation patterns of laminated glass specimens under moderate dynamic loading: (a) predicted, (b) pre-fractured CS2 pinned specimen (test type B), (c) pre-fractured CS3 pinned specimen (test type C) and (d) intact CS2 pinned specimen (test type E). The yellow lines indicate the mid-plane of the specimens in the deformed (solid) and undeformed (dashed) states, with the plastic hinges indicated dotted.

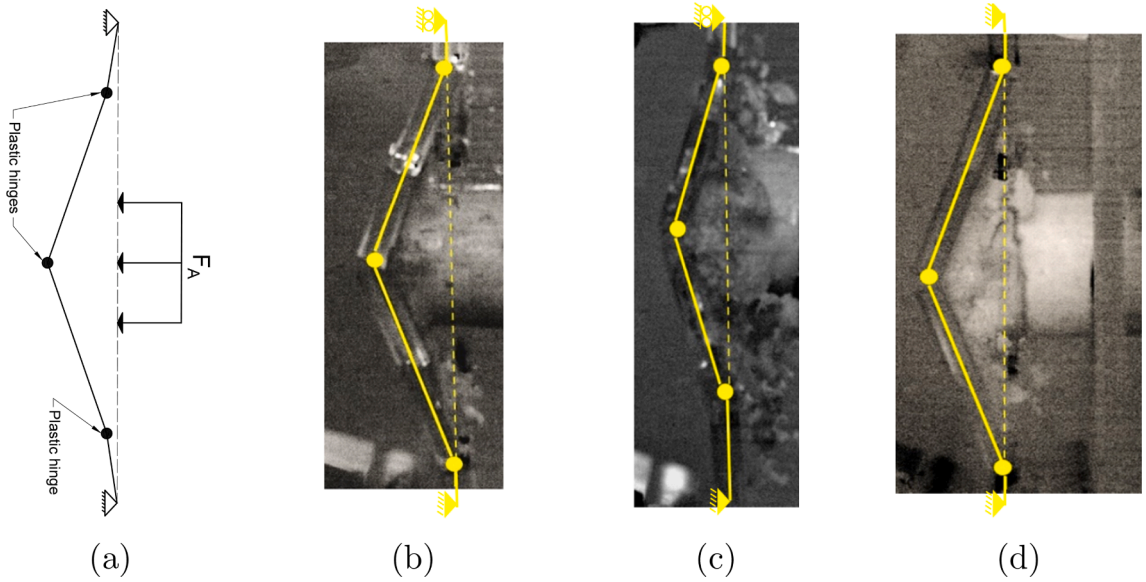

Fig. 23. Comparison of the theoretically predicted and experimentally recorded deformation patterns of laminated glass specimens under intense dynamic loading: (a) predicted, (b) pre-fractured CS1 pinned specimen (test type A), (c) intact CS1 pinned specimen (test type D) and (d) pre-fractured CS1 pinned specimen with axial restraint (test type H). The yellow lines indicate the mid-plane of the specimens in the deformed (solid) and undeformed (dashed) states, with the plastic hinges indicated dotted. Note that the central plastic zone is indicated by straight lines, instead of the curved lines of Fig. 2b, due to the change in loading from uniformly distributed to patch.

Table 4
Comparison of laminated glass failure modes observed with and without axial restraint.

Specimens pre-fractured	Cross-section size	Failure Mode	
		Without axial restraint	With axial restraint
No – intact specimens	CS1	Fracture of both glass plies with subsequent tearing of PVB	Specimens remained intact
Yes – uniform fracture pattern	CS1	PVB tearing	PVB tearing
	CS3	No PVB tearing	No PVB tearing and small displacements

of the PVB, which has a thickness of 0.38 mm in the CS1 specimens. Previous experimental work by Hooper [2] has shown that a minimum PVB thickness of 1.52 mm is required for the delamination front to travel quickly, relieve the interlayer from excessive strains and prevent premature tearing. For specimens with thicker PVB interlayers, such as the pre-fractured CS3 specimens ($h_{PVB} = 1.52$ mm), the introduction of axial restraint results in smaller deflections, as observed in Fig. 20b. This is attributed to the membrane action dominating the response at large deflections. On average, the maximum deflection is reduced to one third of that observed in simple bending.

5. Conclusions

This study has aimed to further our understanding of the blast response of laminated glass by investigating the influence of inertia, which is known to be significant under the accelerations experienced by a panel during a typical blast event. The research aimed to bridge the knowledge gap between the material response under quasi-static loading and full-scale blast testing, as a continuation of previous experimental work that focused solely on the effects of high strain-rate. Laminated glass specimens with a PVB interlayer were impacted with polymer foam projectiles, launched from a gas gun, to simulate the loading from a blast pulse, and the dynamic response recorded with a high-speed camera. Nine different test types were performed by varying the boundary conditions (pinned supports with and without axial restraint), impacting both intact and pre-fractured specimens and testing glass specimens with different cross-section sizes (increasing the thickness of the glass plies and the PVB).

It was found that the collapse mechanisms formed in the specimens under short-duration loading depend on the pulse intensity. For low intensity loading, a single plastic hinge was observed, whereas for high intensity loading (greater than three times the static collapse load) a further two hinges were observed. These observations provide further evidence of the ability of laminated glass to develop plastic hinges, and therefore yield lines, as part of a dynamic, plastic collapse mechanism in which inertia plays a significant role. They provide new insight into the repeated failure pattern observed in blast tests, and help to provide a robust, first-principles justification for the yield line patterns adopted empirically in existing analytical models. Such models, are used for deriving the mid-panel displacement time-history of fractured panels and offer a potential tool for practitioners to make early design predictions of panel capacity without laborious calculations, as well as helping to validate more detailed analyses performed with finite-elements or equivalent single-degree-of-freedom models performed at more detailed design stages. However, further research is required to confirm if the collapse mechanism eventually converges to that observed under moderate dynamic (or quasi-static) loading, resulting in the travelling hinges of standard rigid-plastic theory.

The incorporation of axial restraint led to a significant reduction in the deflection of intact specimens during the impact tests, which remained unfractured. This is consistent with a combined bending and membrane action, which results in lower total longitudinal stresses compared to simple bending. The membrane contribution is also significant in the post-fracture stage, with the maximum deflection of pre-fractured specimens reducing to one third of that observed in simple bending, without axial restraint. However, the benefit of axial restraint was only observed for specimens with PVB thickness greater than 1.52 mm, as thinner interlayers led to premature tearing of the PVB.

Declaration of Competing Interest

The authors declare that they have no known competing financial interests or personal relationships that could have appeared to influence the work reported in this paper.

Data availability

Data will be made available on request.

Acknowledgements

The first author gratefully acknowledges the Engineering and Physical Sciences Research Council for funding this research through the EPSRC Centre for Doctoral Training in Future Infrastructure and Built Environment at the University of Cambridge (EPSRC Grant Reference No. EP/L016095/1). The contribution of the Institution of Civil Engineers, through the ICE Research and Development Enabling Fund, is also gratefully acknowledged. The authors wish to thank Dr Graham McShane of the University of Cambridge for his guidance and advice in designing and performing the gas-gun tests; Kuraray and ToughGlaze for donating some of the glass specimens used in the experiments; and D.J. Goode and Associates Ltd for providing pictures of blast testing of laminated glass specimens.

References

[1] Kranzer C, Gurke G, Mayrhofer C. Testing of bomb resistant glazing systems. In: Glass Processing Days, Tampere, 2005. p. 497-504.
[2] Hooper P. Blast performance of silicone-bonded laminated glass, PhD dissertation, Imperial College London, London, 2011.
[3] Zhang X, Hao H, Wang Z. Experimental study of laminated glass window responses under impulsive and blast loading. Int J Impact Eng 2015;78:1–19. https://doi.org/10.1016/j.ijimpeng.2014.11.020.
[4] Osnes K, Holmen JK, Hopperstad OS, Børvik T. Fracture and fragmentation of blast-loaded laminated glass: An experimental and numerical study. Int J Impact Eng 2019;132:103334. https://doi.org/10.1016/j.ijimpeng.2019.103334.
[5] Angelides SC, Talbot JP. Blast response of laminated glass panels: a critical review of analysis and design methods. In: Proceedings of the Institution of Civil Engineers - Structures and Buildings; 2022. https://doi.org/10.1680/jstbu.20.00248.
[6] Yuan Y, Tan PJ, Li Y. Dynamic structural response of laminated glass panels to blast loading. Compos Struct 2017;182:579–89. https://doi.org/10.1016/j.compstruct.2017.09.028.
[7] Del Linz P, Liang X, Hooper PA, Arora H, Pascoe L, Smith D, et al. A numerical method for predicting the deformation of crazed laminated windows under blast loading. Eng Struct 2018;172:29–40. https://doi.org/10.1016/j.engstruct.2018.05.030.
[8] Angelides SC, Talbot JP, Overend M. The effects of high strain-rate and in-plane restraint on quasi-statically loaded laminated glass: a theoretical study with applications to blast enhancement. Glass Struct Eng 2019;4:403–20. https://doi.org/10.1007/s40940-019-00107-4.
[9] Angelides SC, Talbot JP, Overend M. High strain-rate effects from blast loads on laminated glass: An experimental investigation of the post-fracture bending moment capacity based on time–temperature mapping of interlayer yield stress. Constr Build Mater 2021;273:121658. https://doi.org/10.1016/j.conbuildmat.2020.121658.
[10] Angelides SC, Talbot JP, Overend M. The influence of fracture pattern on the residual blast resistance of laminated glass: an experimental investigation of the post-fracture bending moment capacity based on time-temperature mapping of interlayer yield stress. Glass Struct Eng 2022;7:549–68. https://doi.org/10.1007/s40940-022-00168-y.
[11] Stronge WJ, Yu TX. Dynamic Models for Structural Plasticity. New York, NY: Springer; 1993.
[12] Symonds PS. Large plastic deformations of beams under blast loading, No. AD0025560. Providence, RI: Brown University; 1953. accessed 22/03/20.
[13] Yu TX, Chen FL. The large deflection dynamic plastic response of rectangular plates. Int J Impact Eng 1992;12:605–16. https://doi.org/10.1016/0734-743X(92)90261-Q.
[14] Martin JN, Symonds PS. Mode approximations for impulsively loaded rigid plastic structures, No. AD0621580. Providence, RI: Brown University; 1965. accessed 22/03/20.
[15] Radford DD, Deshpande VS, Fleck NA. The use of metal foam projectiles to simulate shock loading on a structure. Int J Impact Eng 2005;31:1152–71. https://doi.org/10.1016/j.ijimpeng.2004.07.012.
[16] McShane GJ, Radford DD, Deshpande VS, Fleck NA. The response of clamped sandwich plates with lattice cores subjected to shock loading. Eur J Mech A Solids 2006;25:215–29. https://doi.org/10.1016/j.euromechsol.2005.08.001.
[17] Radford DD, Fleck NA, Deshpande VS. The response of clamped sandwich beams subjected to shock loading. Int J Impact Eng 2006;32:968–87. https://doi.org/10.1016/j.ijimpeng.2004.08.007.
[18] Radford DD, McShane GJ, Deshpande VS, Fleck NA. The response of clamped sandwich plates with metallic foam cores to simulated blast loading. Int J Solids Struct 2006;43:2243–59. https://doi.org/10.1016/j.ijsolstr.2005.07.006.
[19] Rathbun HJ, Radford DD, Xue Z, He MY, Yang J, Deshpande V, et al. Performance of metallic honeycomb-core sandwich beams under shock loading. Int J Solids Struct 2006;43:1746–63. https://doi.org/10.1016/j.ijsolstr.2005.06.079.

[20] Rubino V, Deshpande VS, Fleck NA. The dynamic response of clamped rectangular Y-frame and corrugated core sandwich plates. Eur J Mech A Solids 2009;28:14–24. https://doi.org/10.1016/j.euromechsol.2008.06.001.
[21] Russell BP, Liu T, Fleck NA, Deshpande VS. The soft impact of composite sandwich beams with a square-honeycomb core. Int J Impact Eng 2012;48:65–81. https://doi.org/10.1016/j.ijimpeng.2011.04.007.
[22] Karthikeyan K, Russell BP, Fleck NA, O'Masta M, Wadley HNG, Deshpande VS. The soft impact response of composite laminate beams. Int J Impact Eng 2013;60:24–36. https://doi.org/10.1016/j.ijimpeng.2013.04.002.
[23] Angelides SC, Burgan B, Kyprianou C, Rigby SE, Tyas A. EMBlast: A software for rapidly and accurately predicting blast loads on structures. In: In: Proceedings of the 97th Conference on International Committee on Industrial Construction (CICIND); October 2022. p. 82–8.
[24] Chen A, Kim H, Asaro RJ, Bezares J. Non-explosive simulated blast loading of balsa core sandwich composite beams. Compos Struct 2011;93:2768–84. https://doi.org/10.1016/j.compstruct.2011.05.027.
[25] Yandzio E, Gough M. Protection of buildings against explosions (No. SCI P244). Ascot: Steel Construction Institute 1999.
[26] Structures to resist the effects of accidental explosions (No. UFC 3-340-02). US Army Corps of Engineers, 2014.
[27] Glass in building. Basic soda lime silicate glass products Patterned glass (No. BS EN 572-5:2012). London: British Standards Institution, 2012.
[28] Glass in building - Laminated glass and laminated safety glass - Part 2: Laminated safety glass (No. BS EN ISO 12543-2:2011). London: British Standards Institution, 2011.
[29] Angelides SC. Blast Resilience of Glazed Façades: Towards a New Understanding of the Post-Fracture Behaviour of Laminated Glass, PhD dissertation, University of Cambridge, Cambridge, 2022. https://doi.org/10.17863/CAM.87476.
[30] Jones N. Structural Impact, 2nd ed. Cambridge: Cambridge University Press, 2011. https://doi.org/10.1017/CBO9780511820625.